Large-Deformation Behavior and Failure Process of Steel Moment-Resisting Frames Examined by a Shake-Table Test

Martin SOMARRIBA
Candidate for the Degree of Doctor of Engineering
Supervisor: Dr. Taichiro Okazaki
Division of Architecture and Structural Design

Introduction

Steel moment-resisting frames are popular structural systems in seismic areas. However, seismic excitations produce large deformations that eventually lead to member damage, degradation of strength and stiffness, and collapse. Few studies have been conducted in the past to examine the behavior of steel moment-resisting frames to very large deformations, i.e., story drift ratios greater than 0.10 rad. Furthermore, ductile moment-resisting beam-to-column connections are important to achieve good performance against earthquakes. This research studies the behavior of steel moment-resisting frames through cyclic static tests on beam-to column moment connection subassemblages (component-level response) and dynamic shake-table tests of a scaled moment-resisting frame (system-level response). All the specimens in this study used the current detailing of the Japanese construction practice.

Research Background

Most experimental studies on the collapse of steel structures used simplified models. Rodgers et al. [1] showed that large amplitude pulses in the excitation and large number of fractured beam-to-column connections are significant factors leading to collapse. Lignos et al. [2] evaluated the reduction of collapse capacity due to P-Δ effects and component deterioration. Matsumiya et al. [3] conducted cyclic-loading tests of a three-story building using the post-Kobe Japanese design and construction practice completed with composite floor slabs. The frame sustained a maximum story drift ratio of 0.06 rad in the first story before yielding and local buckling of both ends of the first story columns caused a 50% reduction in story shear.

Large shake table tests by Suita et al. [4] subjected a four-story steel building to bidirectional ground motions. After sustaining a story drift ratio of 0.025 rad at the first story, shear strength degradation due to local buckling of the first story columns lead the structure to rest on a perimetral safety system at 0.16 and 0.08-rad story drift ratio in the longitudinal and transverse direction, respectively, and a total loss lateral strength. Despite proportioning the members with a strong column-weak beam ratio of about 1.50, such collapse mode was expected because the no-weld-access-hole detail adopted in the beam-to-column connection would increase the demands in the columns. Based on these tests, Lignos et al. [5] suggested that a strong-column/weak-beam ratio of about 2.0 may improve the collapse capacity and avoid a single-story mechanism.

Beam-to-Column Moment Connections to an I-section Column

An experimental and analytical study was conducted on moment connections to an I-shaped column primarily to fill the gap in knowledge due to the scarce experimental data when I-section columns are used.

Fig. 1 shows the details of the six specimens: three for moment connection to the column flange (F1, F2 and F3) and three for moment connection to the column web (W1, W2, and W3).

Specimen W3 used tougher and stronger SN490B continuity plates. The Specimens were subjected to cyclic loading according to the protocol specified in Section K2 of AISC Seismic Provisions [6].
As shown in a, the F-Specimens exhibited large local buckling deformation of the beam flanges and web. Before local buckling, cracks were detected in the groove weld joining the beam flanges to the column. The cracks formed at the toe of the weld groove at the ends of the beam flange. In Specimen F1, the only F-Specimen without doubler plate, the cracks hardly grew. As shown in b, the cracks in Specimens F2 and F3 propagated straight along the interface between the CJP groove weld and beam flange.

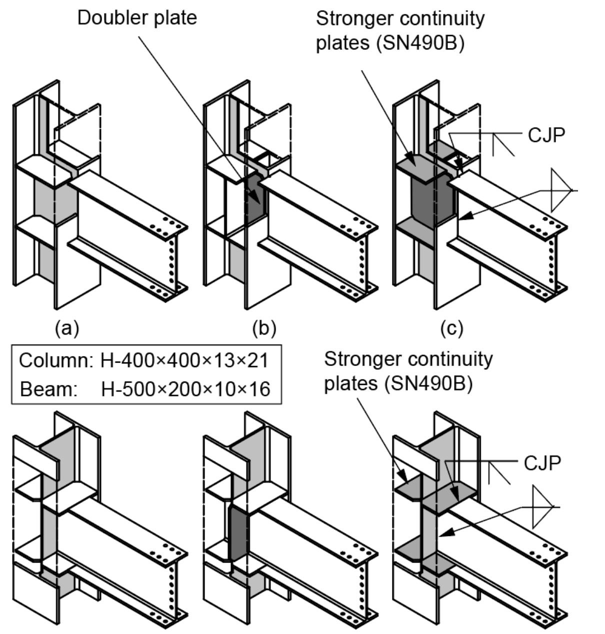

Fig. 1 Beam-to-column moment connection test specimens: a) F1, b) F2, c) F3, d) W1, b) W2, and f) W3.

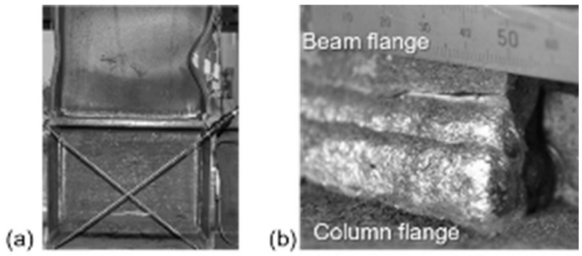

Fig. 2 Observed phenomena in the connections to the column flange: a) local buckling, and b) crack at the groove weld termination.

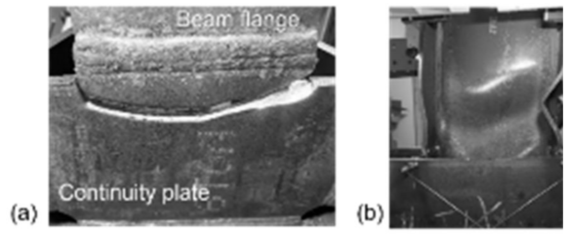

Fig. 3 Observed phenomena in the connections to the column web: a) Fracture of the continuity plate of Specimen W2, and b) local buckling of Specimen W3.

The W-Specimens were prone to fracture of the continuity plate initiating at the termination of the beam flange groove weld, as shown in Fig. 3a. Specimen W2 failed by sudden and complete fracture after that crack developed to about 20% of the width of the beam flange. Specimen W3 formed a very similar crack at the corner between the beam flange and continuity plate, but the cracks did not grow to a substantial size. Specimen W3 formed cracks along the groove of the beam flange, very much like the F-Specimens, which grew to a larger size than the cracks into the continuity plate.

Fig. 4 shows the measured moment at column face versus story drift ratio of the six specimens. Comparing Fig. 4a–c with Fig. 4f, the deformation capacity and strength of the F-Specimens were identical to the W-Specimen which continuity plate did not fracture. Furthermore, all the Specimens except W2 survived the cycles of 0.04-rad story drift ratio while keeping the strength above $0.80M_p$. Therefore, the connections met the ductility requirements for Special Moment Frames per AISC Seismic Provisions. Following the same provisions, W2 can be regarded as Intermediate Moment Frame.

Finite-element-method analysis of each tested specimen was performed using the general-purpose analysis software ADINA Ver.9.6 to further investigate the causes of damage.

Fig. a shows the principal stresses near the critical regions of the connections to the column web, when the beam flange is subject to tension at the first excursion of the ±0.03-rad cycle. At this stage, marked by "▲" in Fig. d and e, the cracks observed in Specimens W1 and W2 propagated rapidly into the continuity plates.

All three web-connection numerical models showed notably high stress at the corner between the beam flange and continuity plate, at the location where all three specimens formed a crack. It is also noted that the large principal stress acted perpendicular to the corner, to open any crack formed at this location, as reported for Specimens W1 and W2. Although little difference in stress distribution was confirmed between the three models, the maximum principal stress was higher in Model W2 (803 N/mm^2) than in Models W1 and W3 (772 and 770 N/mm^2, respectively).

The right corner between the beam flange and continuity plate, as well as cracks formed at this location, act as a notch placed perpendicular to such principal stress. The continuity plates were equal to the beam flanges in thickness. Therefore, it can be seen that the continuity plates in Specimens W1 and W2, which had lower yield strength than the beam flange (293 N/mm^2 compared to 321 N/mm^2) yielded while the continuity plates in Specimen W3, which had higher yield strength than the beam flange (412 N/mm^2 compared to 321

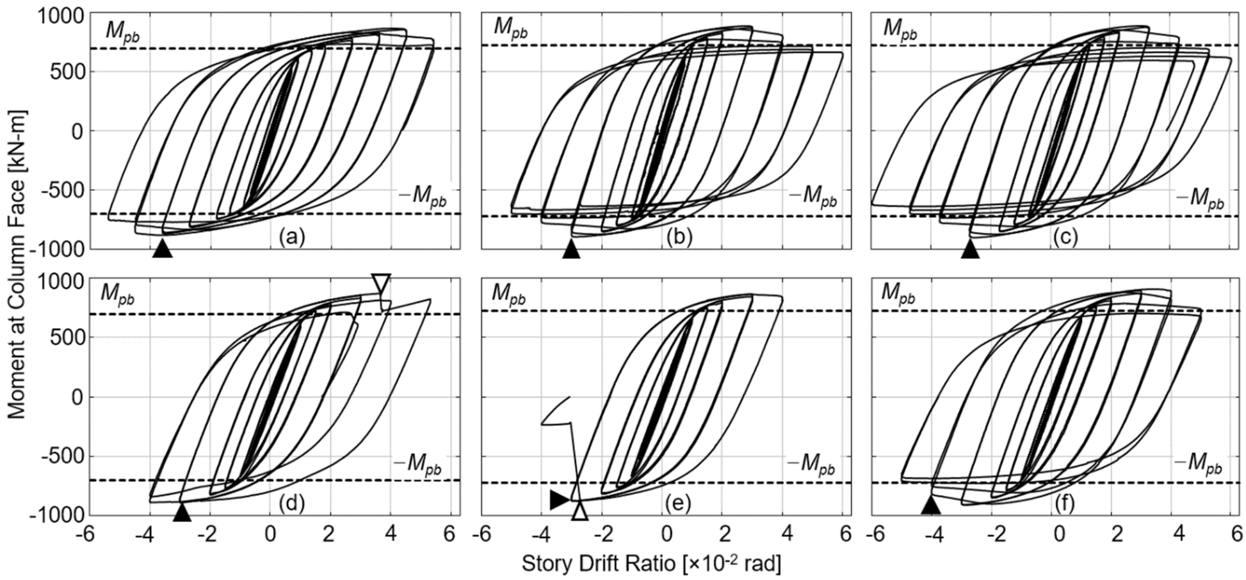

Fig. 4 Response of Specimens: a) F1, b) F2, c) F3, d) W1, e) W2, and f) W3.

N/mm^2) did not yield as substantially. Consequently, the significantly different performance between Specimens W2 and W3 may be attributed to whether the continuity plates yielded during the test.

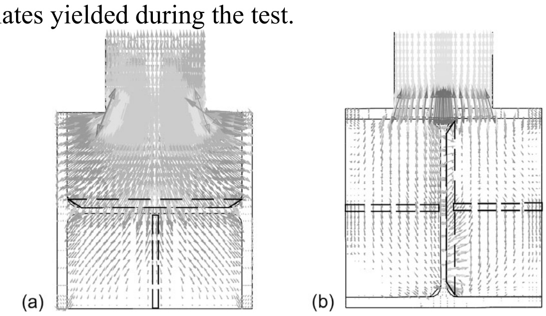

Fig. 5 Principal stresses in: a) W-Specimens, and b) F-Specimens.

Shake-Table Collapse Tests

Test Plan

Fig. 6a shows the elevation of the specimen, which was a 2/5-scale, 2-bay, 4-story steel moment-resisting frame fixed at the column bases. All stories were 1.25 m in height and 3 m in span. Table 1 lists the beams and columns. The columns used JIS (Japanese Industry Standard) STKR designation, cold-formed, square-hollow-structural sections (HSS), and the beams used JIS SS400 I-sections. To supply the targeted inertia, concrete weights, approximately 2.8 ton each, were fastened to the floor beams through high strength PC-rods. The total 50-ton mass of the entire specimen was supported by the main frame and two gravity frames aligned in parallel.

As shown in Fig. 6b, the gravity frames had pinned bases, and their beams were provided with slotted-hole shear connections to minimize lateral load resistance of the gravity frame. Fig. 6c illustrates the rigid diaphragm formed at each floor, connecting the top flange of the beams through turnbuckles, to transfer all inertia to the main frame. As shown in Figs. 6a and 6b, sagged braces were placed in the lower stories which would engage at very large story drifts to protect the shake table from collapse of the specimen. As in the Japanese construction practice of low- to mid-rise steel buildings, beam stubs were shop welded to the columns, and the frame was completed on the site by splicing the central 1500-mm beam segments through high-strength bolts tightened to slip-critical condition.

Fig. 7 details the beam-to-column moment connection adopted in the main frame. The Complete Joint Penetration (CJP) groove welds at the beam flanges did not require weld access holes. First, backing bars split at the beam web were tack-welded inside the beam flange bevel. Next, the beam web was connected to the column by fillet welds. Last, the beam flanges were connected to the diaphragm by CJP groove welds.

Table 1 lists the mechanical properties of steel established from coupon tests. The measured yield strengths were 1.8, 1.7, and 1.3 times the nominal for columns C1 and C2, and beams G1 and G2. The members were proportioned such that the ratio or sum of plastic moments between the column and beam from nominal strength values are 2.3 and 1.1, respectively, for the exterior and interior joints.

The plastic strength between the panel zones and the sum of plastic moments of the beams were 1.7 for the external and 0.8 for the internal joints. However, due to the higher-than-expected strength of the columns, the panel zone-to-beam strength ratio from measured properties resulted in 2.3 and 1.1 for the external and internal joints, respectively.

The JMA Kobe NS record was applied in the plane of the specimen. The motion was gradually increased from 10% to 100%, and the 100% excitation was repeated 4 times.

Uniaxial elastic strain gages were placed on multiple sections of each beam and column to enable sampling of internal force distribution. Strain gages were also placed on the first and second-story columns of the gravity frames. Displacement transducers were placed at each story between the top of the concrete weights or foundation beam and upper beam to measure relative story drift. Displacement transducers were used to measure beam-end rotation, panel-zone shear deformation, and slippage of the column base plates. Uniaxial accelerometers were attached to the concrete masses at each story.

Test Results

Fig. 8 shows the transition of the specimen's first and second natural vibration periods identified from white noise excitations conducted between primary excitations and from the tail of the acceleration t response when white noise was not available. The period remained practically constant even after the 50% excitation when the second and third-floor beams and the column bases yielded substantially as mentioned later. This result suggests that steel systems can retain their elastic properties even after experiencing significant yielding of primary components. The natural period elongated to 0.64 s after the 4th 100% excitation due to fracture of the second-floor beams.

Fig. 9 presents the bending moment distribution normalized by the plastic strength M_p based on strain gauge measurements sampled from the 50%, 1st 100%, 3rd 100%, and 4th 100% excitations at peak deformation. The figure indicates the zone where the plastic strength was exceeded, as well as the locations where the fracture occurred. During the 50% excitation, the second and third-floor beams developed plastic hinges at both ends and the first-story columns yielded at the bases. During the 1st 100% excitation, the system formed a sidesway mechanism involving the lower three stories. Yielding continued to spread during the subsequent 100% motions until the bottom flange of the external joint beams on the second floor fractured. During the 3rd 100% excitation, a crack formed at the termination of the CJP groove weld, at the location indicated in Fig. 10, then propagated along the weld bevel until it rested 25 mm (12% of the beam depth) into the web. During the 4th 100% excitation, the beam bottom flange completely fractured to the state shown in Fig. 8b.

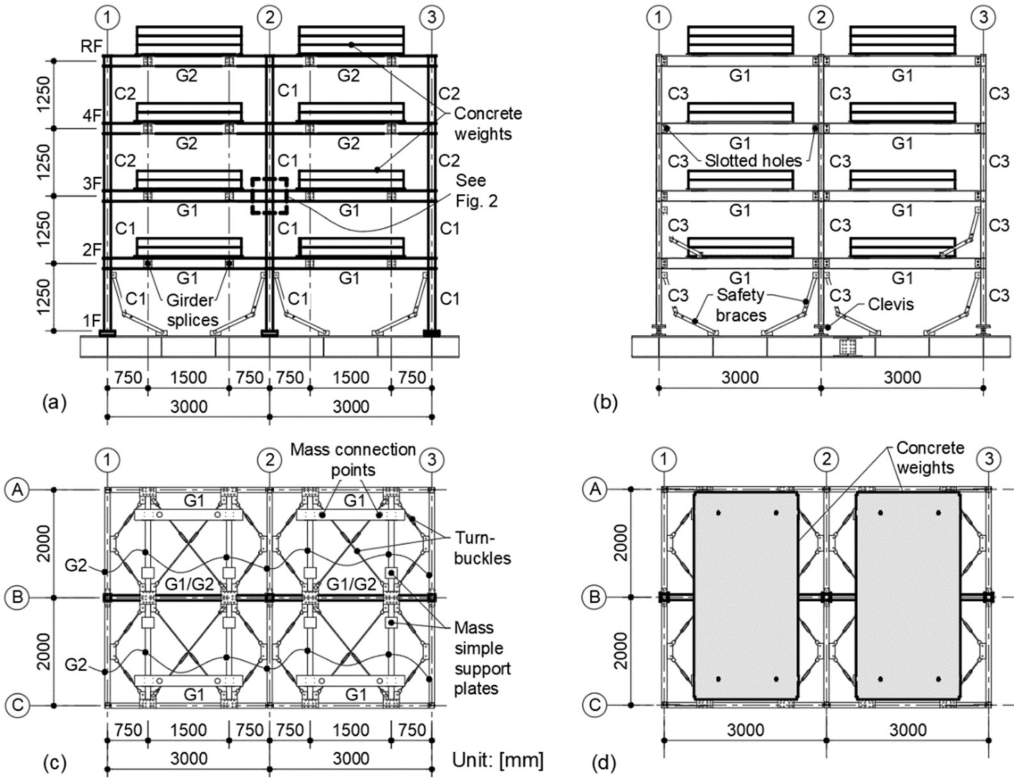

Fig. 6 Test specimen: a) Main frame elevation, b) Gravity frame elevation, c) Floor diaphragm, and d) Placement of concrete weights in plan.

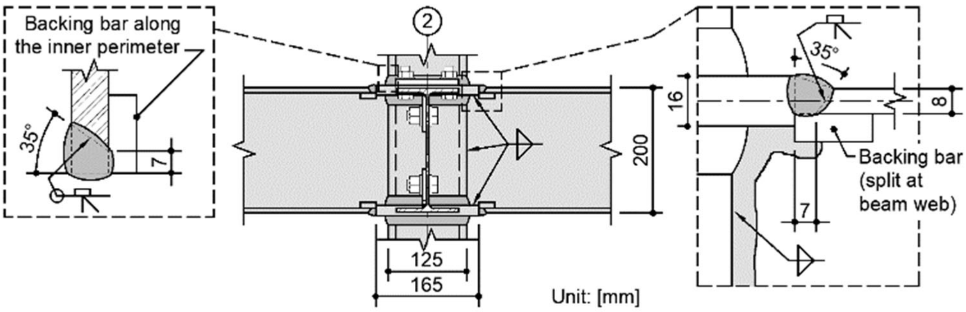

Fig. 7 Beam-to-column moment connection with no weld-access-hole at flange connection.

Table 1 Column and beam schedule and specified minimal mechanical properties.

Member	Dimensions	Grade	F_y [N/mm^2]	F_u [N/mm^2]
C1	HSS-125×125×12	STKR400	245	400
C2	HSS-125×125×9	STKR400	245	400
C3	H-100×100×6×8	SS400	245	400
G1	H-200×100×5.5×8	SS400	245	400
G2	H-198×99×4.5×7	SS400	245	400

Fig. 11a plots the base moment at the central column vs. story drift response of the first story during the four 100% excitations. Despite the large story drift of +0.08 and −0.02 rad induced by each of the 100% excitations, no strength degradation occurred in this column. The normalized P-M interaction in Fig. 11b indicates no significant variation of column axial load for the interior column (−0.07, −0.06P_y), whose initial axial due to gravity loads was 6% of its axial yield strength. The columns exhibited very ductile behavior showing no sign of local buckling and developing no sign of fracture in the CJP groove welds to the column base plate.

Component Tests

Three beam-and-column subassemblages were constructed simultaneously with the shake-table specimen using the same heat of steel, design, and detailing.

As shown in Fig. 12, the subassemblages represented two external joints (T1 and T2) and one internal joint (T3). During the tests, the subassemblages were laterally braced at the same locations where the moment-resisting beams of the shake-table test specimen were braced by orthogonal beams.

The subassemblages were subjected to cyclic loading to a story drift ratio of ±0.05 rad according to the loading protocol for beam-to-column connections defined by the AISC Seismic Provisions Sect. K2. Subsequently, the loading cycles were skewed to one direction to a maximum of −0.125 rad.

Fig. 13 shows the beam-end moment versus beam rotation obtained from the three Specimens. Specimen T3 is represented by the right beam noting that the left beam showed nearly identical behavior but fracture occurred only in the right beam. All specimens behaved similarly. Local buckling of the beam became prevalent during the second +0.05-rad excursion (marked by △), followed by crack initiation in the top beam flange at the termination of the CJP groove weld during the subsequent half cycle (▲). The "×" in Figs. 13b and 13c indicate fracture of the beam top flange of Specimen T2 and the bottom flange of the right beam of Specimen T3.

Fig. 14 shows the same relationships obtained from corresponding beams in the shake-table test during the four 100% JMA Kobe N-S excitations. The shake-table test specimen developed similar flexural strength at the connections and similar damage progression as the subassemblages. However, unlike the subassemblages, the shake-table test specimen exhibited no significant degradation in strength or stiffness before fracture. This

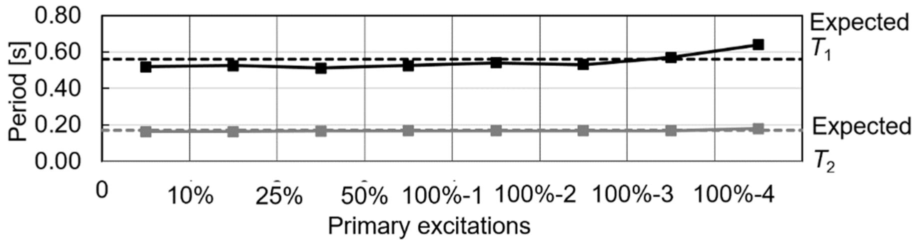

Fig. 8 Variation of the natural period between excitations.

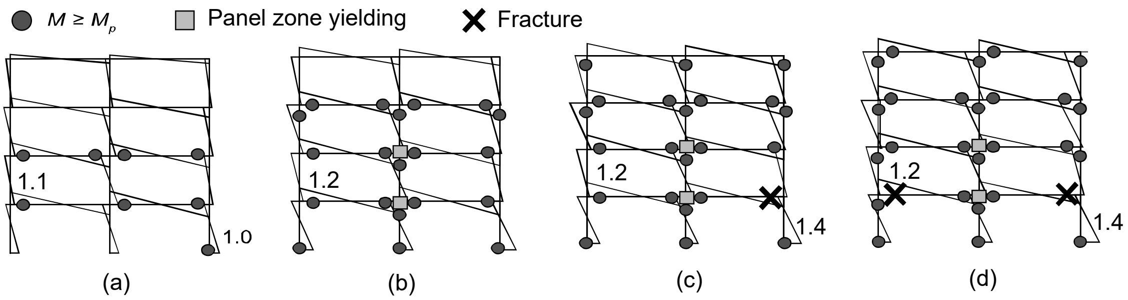

Fig. 9 Normalized bending moment diagram at maximum deformation and damage propagation at the excitations: a) 50%, b) 1st100%, c) 3rd 100%, and d) 4th 100%.

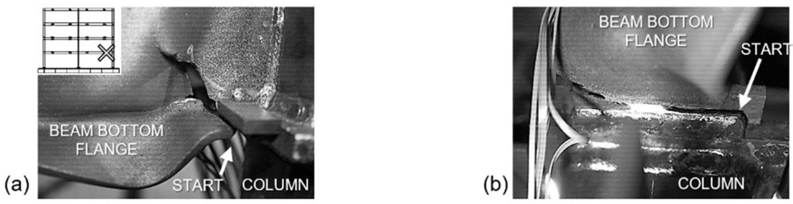

Fig. 10 Fracture of 2F beam at the end of the tests: a) front view, and b) bottom view.

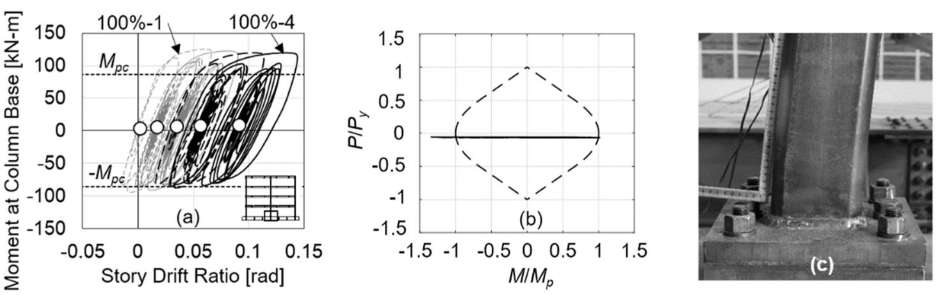

Fig. 11 Response of the interior column base during the 100% excitations: a) Moment at column base vs. story drift ratio, b) P-M interaction, and c) deformation at the end of the tests.

difference may be attributed to the axial restraint of the beam by surrounding members that was present in the shake-table tests but not in the subassemblages.

Conclusions

The conclusions drawn from the shake-table tests of a scaled steel moment-resisting frame and corresponding beam-to-column subassemblages are:

- A strong column/weak beam ratio of 3.0 in the first story joints was adequate to form a sideway plastic mechanism involving the first three stories, as it was predicted in the design process.
- Cracking at the termination of the CJP welds progressed slowly and their effect on either the beam or the system response was not evident until complete fracture of the bottom flange happened.
- Despite sustaining large deformations up to 0.15 rad story drift ratio, the system did not collapse due to the very high strength of the columns.
- The system retained its fundamental period even after the significant yielding of primary components but elongated after beam fracture.
- A comparison of the component tests with the shake-table tests showed good agreement in strength capacity at the beam-to-column connection level but differed in terms of degradation. The difference may be attributed to axial deformation restraint in the shake-table test beams.

References

[1] Rodgers, J. E., Mahin, S. A. Effects of connection fractures on global behavior of steel moment frames subjected to earthquakes. *J Struct Eng* 132(1):78–88. 2006.

[2] Lignos, D. G., Krawinkler, H., Whittaker, A. S. Prediction and validation of sidesway collapse of two scale models of a 4-story steel moment frame. *Earthquake Engng Struct. Dyn.* 40(7):807–825. 2011.

[3] Matsumiya, T., Nakashima, M., Suita, K., Liu, D. Full-scale test of three-story steel moment frames for examination of extremely large deformation and collapse behavior. In: 13th World Conference on Structural Engineering, Vancouver, B.C., Canada. Paper No. 3471. 2004.

[4] Suita, K., Matsuoka, Y., Yamada, S., Shimada, Y., Tada, M., Kasai, K. Experimental procedure and elastic response characteristics of shaking table test. *J Struct Constr Eng* (AIJ) 74(635):157–166. 2009. (In Japanese)

[5] Lignos, D. G., Hikino, T., Matsuoka, Y., Nakashima, M. Collapse assessment of steel moment frames based on E-Defense full-scale shake table collapse tests. *J Struct Eng* 139(1):120-132. 2013.

[6] AISC. Seismic provisions for structural steel buildings. ANSI/AISC 341-22. Chicago, USA. 2022

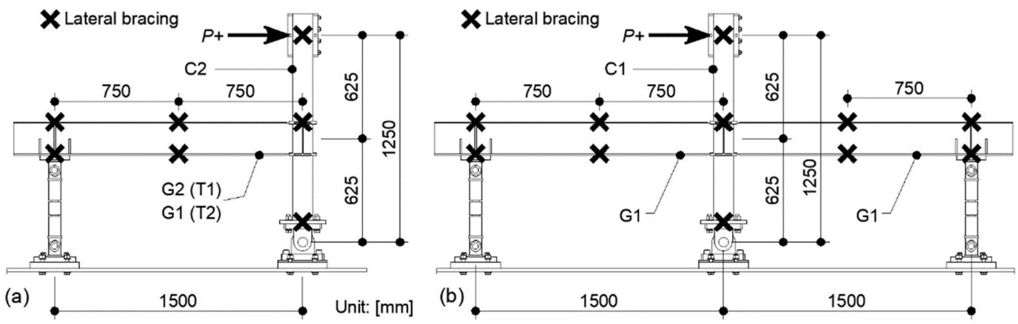

Fig. 12 Beam-to-column subassemblages: a) T1 and T2, and b) T3.

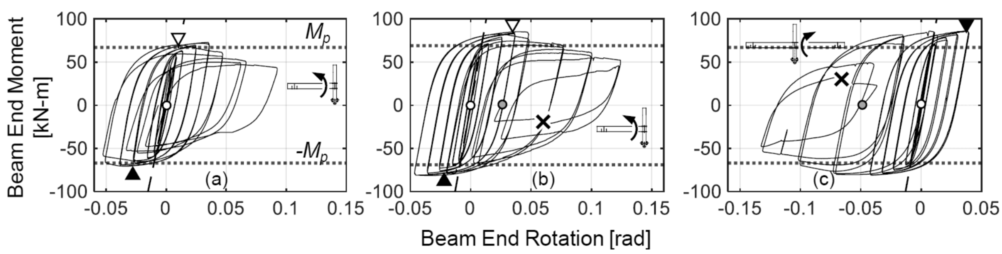

Fig. 13 Beam-end moment vs. rotation response of Specimens: a) T1, b) T2, and c) T3 (right).

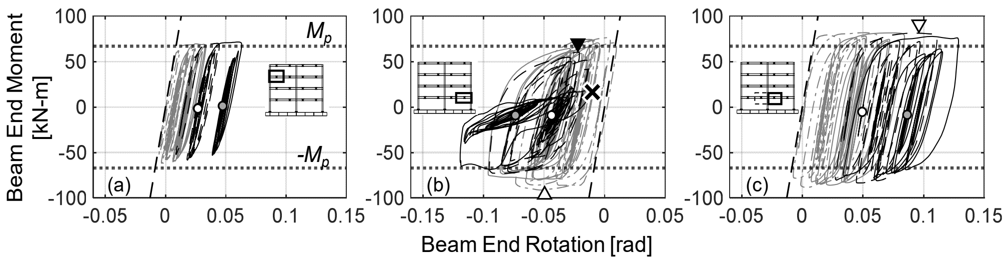

Fig. 14 Beam-end moment vs. rotation response of the shake-table test at: a) 4F external joint, b) 2F external joint, and c) 2F internal joint.